ChemComm

Assessing the Impacts of Dynamic Soft-Template Innate to Switchable Ionic Liquids on Nanoparticulate Green Rust Crystalline Structure

Journal:	*ChemComm*
Manuscript ID	CC-COM-06-2019-004581.R1
Article Type:	Communication

COMMUNICATION

Assessing the Impacts of Dynamic Soft-Template Innate to Switchable Ionic Liquids on Nanoparticulate Green Rust Crystalline Structure

Received 00th January 20xx,
Accepted 00th January 20xx

DOI: 10.1039/x0xx00000x

Jian Zheng,[a] Xiao-Ying Yu, *[b] Manh-Thuong Nguyen,[a] David Lao,[b] Yifeng Zhu,[a] Feng Wang,[c] and David J. Heldebrant*[b]

This experimental and theoretical study investigates how dynamic solvation environments in switchable ionic liquids regulate the composition of nanoparticulate green rust. A custom microfluidic device enables in situ X-ray absorption spectroscopy to elucidate characterization of the solvent structure and speciation of reaction intermediates of air-sensitive nanoparticles growing in solution.

Switchable ionic liquids (SWILs) are a class of green solvents that reversibly switch between ionic and neutral states by means of a chemical trigger gas, most commonly carbon dioxide (CO_2).[1, 2] The first reported SWIL consisting of diazabicyclo [5.4.0]-undec-7-ene (DBU) and 1-hexanol was studied as the archetypical formulation. (Scheme 1) SWILs have been successfully developed for a myriad of applications, ranging from liquid-liquid extractions,[3] separation,[4] and organic synthesis.[5] The ion pairs with organized solvent structure in SWILs can also act as capping agents or "soft templates" for the synthesis of Ag and Au nanoparticles,[6-10] and use as a co-catalyst for combined capture and catalytic conversion of CO_2 to fuels.[11-14]

From a practical application standpoint, DBU:1-hexanol is a green solvent, as it chemically contains up to 15 wt.% CO_2 at 1 atm. that eliminates the need for elevated pressures commonly needed for chemical conversions with CO_2.[15] Further, the hexylcarbonate has been observed to undergo assembly (direct coordination) with the addition of metal complex to form cationic molecular catalysts enabling inner-sphere reactions such as catalytic reduction.[12] The reactivity of anionic carboxylates (e.g., hexylcarbonate) differs substantially from gaseous CO_2, which operates in catalytic reactions via an outer-sphere mechanism, thus opening new approaches for catalyst development based on "captured" CO_2.[16]

We recently mapped the chemical speciation of DBU:1-hexanol using *in situ* liquid time-of-flight secondary ion mass spectrometry (ToF-SIMS), which confirmed a theoretically predicted "heterogeneous" mesoscopic structure, containing disparate regions of ionic and non-ionic solvent, even though stoichiometry would indicate a 100% ionic solvent at full CO_2 loading.[17-20] The size of spherical $[DBUH]^+C_6H_{12}OCO_2^-$ ionic clusters was determined to be approximately 5-20 nm. We hypothesized that the same mesoscopic structures inherent to SWILs would hold the key to the observed reactivity and solvation environment (i.e., soft template) that would solvate catalysts and may keep nanoparticles such as green rust in the nanometer scale during synthesis. When CO_2 is present, $[DBUH]^+C_6H_{12}OCO_2^-$ could preferentially provide a strong polar and ionic solvation medium which the cations and anions would provide charge stabilization of charged ions or polar intermediates formed in nucleation and growth reactions.[7]

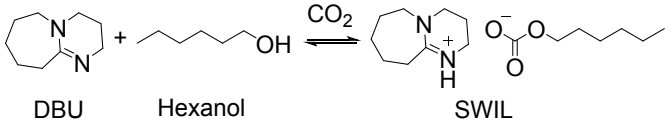

Scheme 1. The reversible formation of ionic liquid from CO_2, 1-hexanol, and DBU

Although it is known that SWILs are a good medium for solvation of catalysts and reagents for chemical transformation and nanoparticle synthesis, little is known as to how and where the chemical reactivity of SWILs arises. This is due to the lack of direct experimental measurements of how the varying structure of SWILs impacts solvation environments, *i.e.,* soft templates for catalytic reactions or nanoparticle nucleation and growth. Characterization of soluble and insoluble species was initially attempted using spectroscopic techniques such as off-line NMR and IR, though neither provided useful information due to paramagnetism and detector saturation, respectively.[21, 22] X-ray absorption spectroscopy (XAS) might be powerful in studying solvation environments[23] to offer the local structural information of the primary solvation spheres of the SWIL during catalysis or the formation (nucleation and growth) of metallic (e.g., Ag, Au, Fe) nanoparticles.

In this study, the archetypical DBH:1-hexanol:CO_2 solvent was chosen. Moreover, $Fe(OAc)_2$ was used as a model surrogate for a molecular catalyst because the Fe precursor has also been shown to produce a nano-green rust.[7] Green rusts (GRs) are a class of highly reactive mineral containing octahedral iron hydroxide layers carrying

[a] *Physical and Computational Sciences Directorate, Pacific Northwest National Laboratory, Richland, WA 99354, USA.*
[b] *Energy and Environment Directorate, Pacific Northwest National Laboratory, Richland, WA 99354, USA. Email: xiaoying.yu@pnnl.gov; david.heldebrant@pnnl.gov*
[c] *Sustainable Energy Technologies Department, Brookhaven National Laboratory, Upton, NY 11973, USA.*
† *Footnotes relating to the title and/or authors should appear here*
Electronic Supplementary Information (ESI) available: [details of any supplementary information available should be included here]. See DOI: 10.1039/x0xx00000x

positive charge and interlayers consisting of anions and water molecules.[24] GRs are of interest as easy to handle reductants used for removal of nitrates from wastewater[25-28] and radioactive contaminants (e.g., U^{4+}, Tc^{7+}) and other metal contaminants (e.g., As^{3+}, Cr^{4+}, Se^{4+}) from solutions.[29-34] Given the air sensitive nature of green rust, it is critical to characterize these systems in its native liquid state as suspended particles, otherwise the solvent and catalyst surrogate/nanocrystalline green rust would undergo changes during isolation and analysis.[24] Thus, we employed a transferrable microfluidics, System for Analysis at the Liquid Vacuum Interface (SALVI), to enable the probing of solvation of a model molecular catalyst in addition to solvation and growth of green rust as it is being made in SWIL.[35] The microchannel reactor was designed to provide a medium for *in situ* XAS analysis (Figure S1).[23] The SALVI microfluidic reactor provides an unprecedented level of understanding of solvation environments and growth mechanisms of catalyst solvation within the SWIL, rather than post-mortem analysis as is commonly done in nanoparticle synthesis. The addition of density functional theory (DFT), enables assessment of the electronic structures of previously unidentified chemical precursors and key reaction intermediates for the synthesis nanocrystalline green rust as a function of the solvation environment by means of different ionic or non-ionic states of the SWIL.

Three liquid mixtures and the final GR precipitate were studied to probe the solvent effect on the structure of ionic and non-ionic clusters and the GR crystalline in addition to chemical transformation. $Fe(OAc)_2$ was initially dissolved in an anhydrous mixture of DBU and 1-hexanol (**1**, light brown solution, Figure S2) to study solvation and speciation of Fe in the non-coordinating form of the SWIL. With the addition of CO_2 as an acidic trigger gas, the solution was converted into its ionic form (**2**, near colorless solution) to study changes in solvation and speciation of Fe in an ionic and strongly coordinating form of the SWIL. Methanol was then added as an oxidant (Schikorr reaction)[36] to observe changes in speciation and solvation of Fe after oxidation from Fe(II) to Fe(III). The green solution (**3**), contains a large fraction of Fe (III) species that are assumed to be the precursors of nano green rusts. It is precipitated out of the solution by changing the solvation environment in SWIL by removing CO_2 (**4**).[7]

The samples were subjected to XANES measurements in real time within the microfluidic device. The spectra are shown in (Figure S3). The position and shape of rising edge and the pre-edge features were used as indicators to determine the oxidation state of the absorbing metal and the geometry of the coordination sphere. The rising edge position of **1** and **2** are similar, while a shift by ~ 2.0 eV higher is observed in **3** and **4**, which indicates the increase of a positive charge on the Fe center in **3** and **4**. This is in agreement with that Fe in **1** and **2** is in the form of Fe (II), which was oxidized into Fe (III) in **3** and **4** as the addition of methanol. We also note a strong pre-edge peak (7111.3 eV) for **1** and weak feature (7112.8 eV) for **2** and **3**, respectively. These observations suggest that tetrahedral coordination in **1** and square planar or octahedral symmetries in **2** and **3**.[37] By comparing the χ(R) EXAFS spectra of the solutions, we note that the bond distance for the first shell coordinator of **1** is ~0.1 Å shorter than those of **2, 3 and 4** (Figure S4). The data are consistent with the SWIL being converted into the ionic form (by sparging with CO_2). It is worth noting that N was replaced by O in the first shell of central Fe.

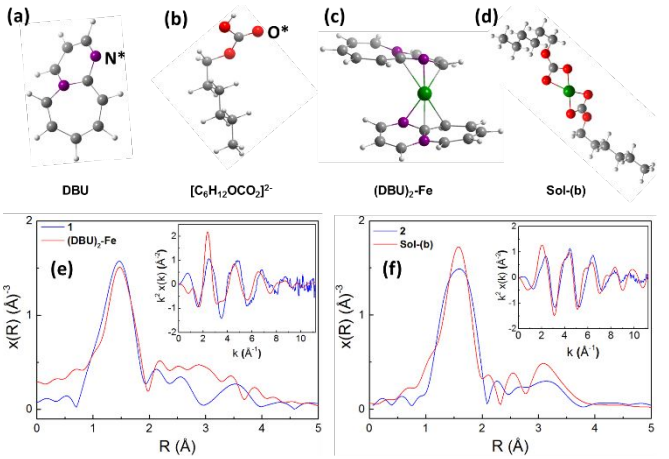

Figure 1. Structure scheme of (a) DBU molecule and (b) $C_6H_{12}OCO_2^{2-}$; N* and O* indicate the bonding sites for Fe; DFT optimized structures of (c) $(DBU)_2$-Fe and (d) Sol-(b), Green, purple, red, grey and white spheres represent Fe, N, O, C and H atoms, respectively; Comparison of Fe k-edge EXAFS χ(R) spectra for (e) **1** and $(DBU)_2$-Fe, (f) **2** and Sol-(b); Insets show the respective x(k) plots.

DFT calculations and FEFF simulations were performed to gain insight into the structure of Fe species in SWILs at the atomic level. A series of computationally optimized models for the non-ionic and ionic solvent were investigated, with the calculated binding energies and relative energies listed in Figures S5-S6 and Tables S1-S2. Although the computed energies can help identify the likely structures of metal-organic compounds to strengthen the findings, we also compared predicted structural parameters with their experimental counterparts. For this comparison, EXAFS spectra of DFT optimized models are generated by using FEFF9 code (see SI for details).[38] The analysis was first done on detectable species in the non-ionic solvent **1**. The best matched model is [$(DBU)_2$-Fe], which corresponds to two DBU molecules coordinated to Fe (Figures 1c, 1e). In this structure, one N atom and two C atoms from each DBU bind to the Fe, with average bond distances of Fe-N and Fe-C of 1.9 and 2.1 Å, respectively. The geometry is composed of two distorted tetrahedrons. In the ionic $[DBUH]^+$ $C_6H_{12}OCO_2^-$ solution **2**, the model Sol-(b) provides the best correspondence to the experimental data (Figures 1d, 1f). This model has the Fe atom bridged to two hexylcarbonate anions via 4 O atoms with an average Fe-O distance of ~2.0 Å to form a distorted planar coordination. We also note that Fe in liquid **3** is still solvated at the molecular level, resembling the structure of Fe in the FeOOH (e.g. lepidocrocite) (Figure S7). The only difference lies in that the Fe-Fe scattering in the χ(R) EXAFS spectra for **3** is much weaker than that of FeOOH. (Figures S7a, S7c). Our results suggest that a solvated FeOOH-like iron species in **3** might be the chemical precursor of green rust, and that Fe-Fe bonds are not formed until the precipitation of the green rust particles during the removal of CO_2 from the SWIL. These findings shed new light on a mechanism of green rust formation. Although there are several works on the *in situ* analysis of the transformation of synthesized GR.[39-41] This study, to the best of our knowledge, has been the first *in situ* observation of the chemical speciation of green rust at various stages of synthesis ionic liquids by XAS.

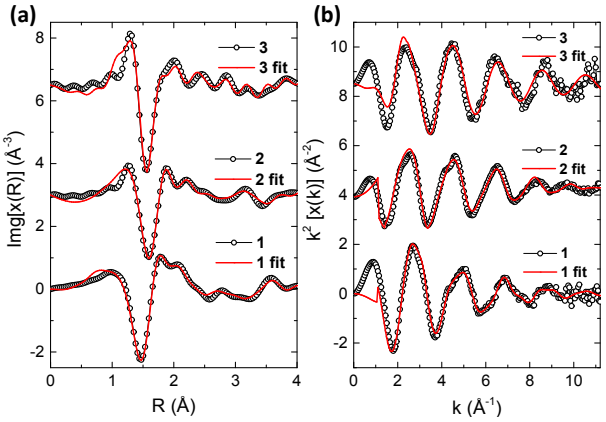

Figure 2. The experimental (black dotted) and fitted (red solid) (a) k^2-weighted Img[χ(R)] and (b) k^2-weighted x(k) spectra of **1**, **2**, and **3**. Spectra are offset along the y-axis for better visualization.

Table 1. The fitting results of Fe K-edge EXAFS

Parameter [a]	1	2	3
CN $_{Fe-N (O)}$ [b]	2.1 (3)	4.3 (6)	6.1 (6)
R $_{Fe-N (O)}$ (Å)	1.868 (3)	2.049 (9)	1.960 (13)
DWF $_{Fe-N (O)}$	0.009 (2)	0.010 (2)	0.004 (2)
CN $_{Fe-C}$	4.4 (9)	2.3 (8)	1.5 (6)
R $_{Fe-C (Å)}$	1.986 (33)	2.496 (24)	2.696 (35)
DWF $_{Fe-C}$	0.008 (1)	0.006 (5)	0.011 (8)
CN $_{Fe-Fe}$	NA [c]	NA	0.5 ± (2)
R $_{Fe-Fe (Å)}$	NA	NA	3.219 (21)
DWF $_{Fe-Fe}$	NA	NA	0.0072 (39)

[a] CN = coordination number, R = interatomic distance, DWF = Debye–Waller Factor; [b] First shell Fe-N path for **1** and first shell Fe-O path for **2** and **3**; [c] NA = not available; Other parameters: E_0 and amp (amplitude reduction factor) are set to the value of Fe_2O_3 reference of -2.3 and 0.84; R-factors < 0.01. The fit is obtained using k-weighting of 2 in the k range of 2.0 Å^{-1} < k < 11.0 Å^{-1}.

The experimental EXAFS spectra of Fe species were fitted with the DFT optimized models, to determine the coordination environment of the Fe clusters in different states of the SWIL. The results are shown in Figure 2 and Table 1. The Fe-N and Fe-C coordination numbers (CN) in the initial DBU solution (**1**) are 2.1 and 4.4, respectively. The fitting results are in good agreement with the DFT predictions, only the corresponded Fe-N and Fe-C distances of 1.87 and 1.99 Å are slightly shorter than that of $(DBU)_2$-Fe model. In ionic liquid **2**, after CO_2 sparging, Fe is coordinated with four O atoms to form a distorted square planar configuration, with an average Fe-O distance of ~2.05 Å, which is in line with the DFT optimized model. No Fe-Fe paths are detected in **1** and **2**. For **3**, the fitted results show that the CN for the first shell Fe-O increases to 6 and the Fe-O distance is 1.96 Å. The fitting quality was improved by including a Fe-C path (CN = 1.5(± 0.6), R = 2.7 Å), which indicates that there is one or two hexylcarbonate sitting in the second shell. These observations are consistent with the hypothesis that cationic catalysts or metal precursors would preferentially dissolve in the soft template (ionic regions) within the SWIL. The data also suggests that there is a Fe-Fe path with CN of 0.5 and a distance of ~3.22 Å. This observation implies that the majority of Fe species in **3** are solvated and would remain so until CO_2 is removed from the SWIL, promoting precipitation and Fe-Fe bond formation. This finding matches the result of our previous experimentally synthesized nano-particulate green rust.[7]

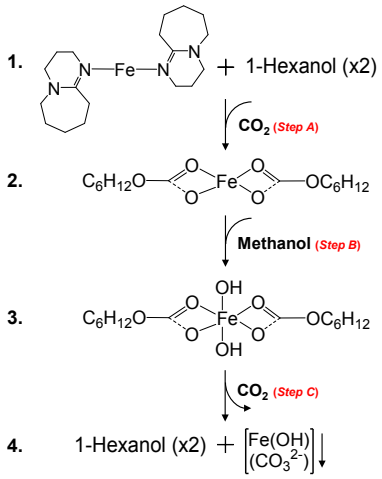

Scheme 2. Proposed reactions during the formation of green rust nanocrystalline in SWILs.

The XANES and EXAFS data, coupled with DFT calculations, have enabled the assessment of how changes in the solvation environment of the SWIL can greatly influence solvation environments and the synthesis of green rust nanoparticles. As depicted in Scheme 2, in the initial non-ionic solvent, Fe binds to the N atoms from the amidine moiety of two DBU molecules. The addition of 1-hexanol and CO_2 changed the SWIL to its ionic form (Scheme 2, Step A), promoting ligand exchange where two $C_6H_{12}OCO_2^-$ displace the DBU molecules, producing a square planar Fe (II) complex with an Fe atom bridged to two hexylcarbonates. This intermediate is structurally similar to the catalyst surrogate and chemical precursor, $Fe(OAc)_2$. This complex was confirmed by both EXAFS and DFT results. Oxidation of the complex via the addition of methanol converts the square planar Fe (II) complex to an octahedral Fe (III) FeOOH complex (Scheme 2, Step B). EXAFS data suggest that the two hexylcarbonates in the coordination sphere should be intact and in a plane, with two hydroxyl ligands that are opposite to each other. This Fe(III) complex is hypothesized to be the chemical precursor of nanoparticulate green rust, as the planes of carbonate and hydroxide could grow head to tail after CO_2 is removed from the SWIL, promoting growth of the observed layered Fe hydroxy-carbonate structure inherent to green rust (Scheme 2, Step C).[7]

In conclusion, we report a new strategy to study the dynamic solvation environments within SWILs using nanoparticulate green rust as a model system. In this work, we newly identified structural progression from linear, square planar, then ultimately octahedral iron complexes as reaction intermediates predicted on integrative XAS measurements and DFT calculations. We propose that the solvated octahedral Fe hydroxide complex is a critical intermediate for nucleation and growth of nanoparticulate green rust upon removal of CO_2 from the SWIL. Our findings provide new insight into how the CO_2-activated dynamic solvent environment innate to SWILs can be used as a soft template for synthesis of nanoparticles (including but not limited to Ag or Au) or catalytic reactions. Ultimately, the design, fabrication, and validation of data collected from SALVI opens up the possibility to perform *in situ* probing of

solvent and solvation effects of air sensitive liquids and understanding the nanocrystalline structure of soluble species in a liquid medium.

Acknowledgement

We thank the United States Department of Energy's Office of Science Basic Energy Sciences Early Career Research Program FWP 67038 for funding. Pacific Northwest National Laboratory (PNNL) is operated by Battelle for the DOE under Contract DE-AC05-76RL01830. Computational resources were provided through allocation at the National Energy Research Scientific Computing Center (NERSC) located at Lawrence Berkeley National Laboratory. We thank Wei Zhang and Bingwen Liu for their technical support to this work. We acknowledge helpful comments and suggestions regarding XAFS analysis from John Fulton. The use of the National Synchrotron Light Source (X18 A beamline) at the Brookhaven National Laboratory was supported by the U.S. DOE, Office of Science, Basic Energy Sciences, under Contract No. DE-SC0012704.

Conflicts of interest

There are no conflicts to declare.

References

1 P. G. Jessop, D. J. Heldebrant, X. W. Li, C. A. Eckert and C. L. Liotta, *Nature*, 2005, **436**, 1102-1102.
2 P. G. Jessop, S. M. Mercer and D. J. Heldebrant, *Energ Environ Sci*, 2012, **5**, 7240-7253.
3 K. N. Onwukamike, T. Tassaing, S. Grelier, E. Grau, H. Cramail and M. A. R. Meier, *Acs Sustain Chem Eng*, 2018, **6**, 1496-1503.
4 V. M. Blasucci, R. Hart, P. Pollet, C. L. Liotta and C. A. Eckert, *Fluid Phase Equilibria*, 2010, **294**, 1-6.
5 S. G. Khokarale, T. Le-That and J. P. Mikkola, *Acs Sustain Chem Eng*, 2016, **4**, 7032-7040.
6 A. L. Ethier, E. C. Hart, S. R. Saunders, E. J. Biddinger, A. Z. Fadhel, C. Dilek, P. Pollet, C. A. Eckert and C. L. Liotta, *Green Materials*, 2014, **2**, 54-61.
7 D. Lao, R. K Kukkadapu, L. Kovarik, B. W Arey, D. J Heldebrant and S. K Nune, *Current Inorganic Chemistry*, 2016, **6**, 92-99.
8 K. Bryant, G. Ibrahim and S. R. Saunders, *Langmuir*, 2017, **33**, 12982-12988.
9 S. R. Saunders and C. B. Roberts, *Nanotechnology*, 2009, **20**.
10 S. R. Reynolds, K. A. Markland, J. Rood, E. Leonard and S. R. Saunders, *Rsc Adv*, 2016, **6**, 78496-78504.
11 M. Yadav, J. C. Linehan, A. J. Karkamkar, E. van der Eide and D. J. Heldebrant, *Inorganic Chemistry*, 2014, **53**, 9849-9854.
12 D. B. Lao, B. R. Galan, J. C. Linehan and D. J. Heldebrant, *Green Chem*, 2016, **18**, 4871-4874.
13 J. Kothandaraman, R. A. Dagle, V. L. Dagle, S. D. Davidson, E. D. Walter, S. D. Burton, D. W. Hoyt and D. J. Heldebrant, *Catal Sci Technol*, 2018, **8**, 5098-5103.
14 J. R. Switzer, A. L. Ethier, K. M. Flack, E. J. Biddinger, L. Gelbaum, P. Pollet, C. A. Eckert and C. L. Liotta, *Ind Eng Chem Res*, 2013, **52**, 13159-13163.
15 D. J. Heldebrant, C. R. Yonker, P. G. Jessop and L. Phan, *Energy & Environmental Science*, 2008, **1**, 487-493.
16 J. Leclaire and D. J. Heldebrant, *Green Chem*, 2018, **20**.
17 X. Y. Yu, J. Yao, D. B. Lao, D. J. Heldebrant, Z. H. Zhu, D. Malhotra, M. T. Nguyen, V. A. Glezakou and R. Rousseau, *J Phys Chem Lett*, 2018, **9**, 5765-5771.
18 Y. F. Zhou, J. Yao, Y. Z. Ding, J. C. Yu, X. Hua, J. E. Evans, X. F. Yu, D. B. Lao, D. J. Heldebrant, S. K. Nune, B. Cao, M. E. Bowden, X. Y. Yu, X. L. Wang and Z. H. Zhu, *J Am Soc Mass Spectr*, 2016, **27**, 2006-2013.
19 J. Yao, D. B. Lao, X. Sui, Y. F. Zhou, S. K. Nune, X. Ma, T. P. Troy, M. Ahmed, Z. H. Zhu, D. J. Heldebrant and X. Y. Yu, *Phys Chem Chem Phys*, 2017, **19**, 22627-22632.
20 20. D. C. Cantu, J. Lee, M. S. Lee, D. J. Heldebrant, P. K. Koech, C. J. Freeman, R. Rousseau and V. A. Glezakou, *Journal of Physical Chemistry Letters*, 2016, **7**, 1646-1652.
21 H. Shi, J. A. Lercher and X. Y. Yu, *Catal Sci Technol*, 2015, **5**, 3035-3060.
22 G. N. La Mar, W. D. Horrocks and R. H. Holm, *NMR of paramagnetic molecules: principles and applications*, Elsevier, 2016.
23 J. Zheng, W. Zhang, F. Wang and X. Y. Yu, *J Phys-Condens Mat*, 2018, **30**.
24 M. Usman, J. M. Byrne, A. Chaudhary, S. Orsetti, K. Hanna, C. Ruby, A. Kappler and S. B. Haderlein, *Chem Rev*, 2018, **118**, 3251-3304.
25 M. Etique, A. Zegeye, B. Gregoire, C. Carteret and C. Ruby, *Water Res*, 2014, **62**, 29-39.
26 D. Guerbois, G. Ona-Nguema, G. Morin, M. Abdelmoula, A. M. Laverman, J. M. Mouchel, K. Barthelemy, F. Maillot and J. Brest, *Environ Sci Technol*, 2014, **48**, 4505-4514.
27 C. Ruby, C. Upadhyay, A. Gehin, G. Ona-Nguema and J. M. R. Genin, *Environ Sci Technol*, 2006, **40**, 4696-4702.
28 H. C. B. Hansen, C. B. Koch, H. NanckeKrogh, O. K. Borggaard and J. Sorensen, *Environ Sci Technol*, 1996, **30**, 2053-2056.
29 S. E. Pepper, D. J. Bunker, N. D. Bryan, F. R. Livens, J. M. Charnock, R. A. D. Pattrick and D. Collison, *J Colloid Interf Sci*, 2003, **268**, 408-412.
30 P. Refait, L. Simon and J. M. R. Genin, *Environ Sci Technol*, 2000, **34**, 819-825.
31 D. L. Bond and S. Fendorf, *Environ Sci Technol*, 2003, **37**, 2750-2757.
32 L. L. Skovbjerg, S. L. S. Stipp, S. Utsunomiya and R. C. Ewing, *Geochim Cosmochim Ac*, 2006, **70**, 3582-3592.
33 G. Ona-Nguema, G. Morin, Y. H. Wang, N. Menguy, F. Juillot, L. Olivi, G. Aquilanti, M. Abdelmoula, C. Ruby, J. R. Bargar, F. Guyot, G. Calas and G. E. Brown, *Geochim Cosmochim Ac*, 2009, **73**, 1359-1381.
34 E. J. O'Loughlin, S. D. Kelly, R. E. Cook, R. Csencsits and K. M. Kemner, *Environ Sci Technol*, 2003, **37**, 721-727.
35 Y. Z. Ding, Y. F. Zhou, J. Yao, C. Szymanski, J. Fredrickson, L. Shi, B. Cao, Z. H. Zhu and X. Y. Yu, *Anal Chem*, 2016, **88**, 11244-11252.
36 R. M. Cornell and U. Schwertmann, *The iron oxides: structure, properties, reactions, occurrences and uses*, John Wiley & Sons, 2003.
37 T. E. Westre, P. Kennepohl, J. G. DeWitt, B. Hedman, K. O. Hodgson and E. I. Solomon, *J Am Chem Soc*, 1997, **119**, 6297-6314.
38 J. Zheng, J. Ye, M. A. Ortuño, J. L. Fulton, O. Y. Gutiérrez, D. M. Camaioni, R. K. Motkuri, Z. Li, T. E. Webber, B. L. Mehdi, N. D. Browning, R. L. Penn, O. K. Farha, J. T. Hupp, D. G. Truhlar, C. J. Cramer and J. A. Lercher, *J Am Chem Soc*, 2019, **141**, 9292-9304.
39 S. Fujieda, A. Yoshino, K. Shinoda, Y. Takahashi and S. Suzuki, *Isij Int*, 2014, **54**, 125-130.
40 A. Sumoondur, S. Shaw, I. Ahmed and L. G. Benning, *Mineral Mag*, 2008, **72**, 201-204.
41 41. I. A. M. Ahmed, L. G. Benning, G. Kakonyi, A. D. Sumoondur, N. J. Terrill and S. Shaw, *Langmuir*, 2010, **26**, 6593-6603.